The Hubble Space Telescope: 21 years and counting

N. Panagia[1,2,3]

[1] Space Telescope Science Institute, 3700 San Martin Drive, Baltimore, MD 21218, USA
[2] Istituto Nazionale di Astrofisica – Osservatorio Astrofisico di Catania, Via S. Sofia 78, I-95123 Catania, Italy
[3] Supernova Ltd, OYV #131, Northsound Road, Virgin Gorda, British Virgin Islands
e-mail: `panagia@stsci.edu`

Abstract. I summarize the current status of the Hubble Space Telescope (*HST*) and illustrate some of its exciting results.

Key words. Telescopes: HST – Cosmology: observations – Dark Matter – Early Universe – Galaxies: Magellanic Clouds – Stellar Populations – Stars: V838 Mon – Planetary System – Comet: SL9 – Planets and Satellites: Pluto

1. Introduction

After twenty one years in orbit, the now "adult" Hubble Space Telescope (*HST*) continues to play a major role in astronomical research, and is undoubtedly one of the most important and most prolific space astronomy missions of all time.

HST was deployed in low-Earth orbit (about 600 km) by the crew of the space shuttle Discovery (STS-31) on 25 April 1990. Although at the beginning the mission looked severely faulted because of spherical aberration, the first maintenance mission (STS-61 Endeavour, December 1993) fully restored the functionality of *HST*. In fact, all *HST* servicing missions so far, namely SM1 in December 1993, SM2 in February 1997, SM3A in December 1999, and SM3B in February-March 2002 were enormous successes.

Send offprint requests to: N. Panagia

After SM3B, *HST*'s science instruments included a spectrograph, the Space Telescope Imaging Spectrograph (STIS) operating in the UV and optical domains, and three cameras, the Wide Field - Planetary Camera 2 (WFPC2), the Advanced Camera for Surveys (ACS), the Near Infrared Camera - Multiobject Spectrograph (NICMOS), which was revived in mission 3B with the installation of a mechanical cooling system, and the Fine Guidance Sensors (FGS, primarily used for astrometric observations).

However, STIS stopped operations in August 2004, leaving *HST* without a proper spectrographic capability, and ACS failed in January 2007, leaving in operation rather old instruments. Subsequently, *HST* suffered a serious malfunction on September 27, 2008, with a failure of the Science Instrument/Control & Data Handling system, which prevented data from the science instruments being transmitted to the ground. On October 15, 2008,

HST switched to operations on the redundant side of the data transmission system, and later resumed science observations with Wide-Field Planetary Camera 2 (WFPC2) and the Advanced Camera for Surveys Solar Blind channel (ACS/SBC).

Triumphally, in mid-Spring 2009 *HST* was reborn with the Servicing Mission 4 (SM4).

Originally, SM4 was planned for 2004, but was postponed after the Columbia Space Shuttle tragedy in 2003 and then canceled in light of Agency safety concerns. Following the successful recovery of the Shuttle program and a re-examination of SM4 risks, NASA approved one last servicing mission. The reinstated SM4 was initially scheduled for flight in Fall 2008, but, after the failure of a side of the data transmission system, it was postponed to late Spring 2009.

On May 11, 2009, SM4 (STS125) started with the shuttle Atlantis taking seven astronauts to reach the HST, do all repairs and new installations on the telescope in five very intense EVA (ExtraVehicular Activity) sessions, and come back safely on May 24, 2009.

The two new cutting-edge instruments that enhance Hubble's capabilities by large factors, are the Cosmic Origins Spectrograph (COS) and the Wide Field Camera 3 (WFC3). Astronauts also succeeded in the first ever on-orbit repair of two existing instruments - both STIS and ACS. A refurbished Fine Guidance Sensor has replaced one degrading unit of three now onboard, and will maintain a robust ability to point the telescope. In addition, new gyros, batteries and thermal blankets were installed to ensure Hubble functions efficiently for a minimum of five, and possibly ten years after servicing.

2. *HST* results

In 21 years HST has made more than 1,000,000 observations, obtaining almost 500,000 images of about 30,000 different fields.

Observations made with the *HST* have either solved problems that had been under debate for many years, or have revealed quite unexpected and exciting new phenomena.

Among the *HST* high impact science we can mention the definitive measurement of the expansion rate of the Universe, the so-called Hubble constant, the confirmation and characterization of massive black holes in the centers of galaxies, the detection of the host galaxies of QSOs, and the exhaustive study of the properties of the intergalactic medium that tell us about the chemical evolution of the Universe.

Even more exciting are the discoveries that were totally unanticipated and that have opened new avenues to our knowledge of the cosmos, such as the discovery of the acceleration of the Universe, which may imply the existence of the so-called "dark energy" that has been dominating the expansion of the Universe in the last 8 billion years (*e.g.,* Panagia 2005a), the properties of extremely distant galaxies as shown by the Hubble Deep Fields, as well the Hubble Ultra-Deep Field observations that have provided us the direct view at thousands of galaxies formed just a few hundred million years after the Big Bang, clues to the nature of gamma-ray burst sources that are possibly the most energetic explosions in the Universe, the formation of planets in disks around young stars, the full characterization of planets orbiting around other stars but our own Sun, and the dramatic collision of comet Shoemaker-Levy 9 fragments with Jupiter's atmosphere.

With so many exciting results, one should write a thick book to do justice to all of them and to the other many important discoveries that *HST* has enabled us to make. Here, I shall highlight some of the recent discoveries made possible by Hubble. Summaries of previous years most exciting *HST* results may be found in Panagia (1999, 2005b, 2010).

3. Cosmology and the distant Universe

3.1. The evolution of galaxies and the cosmic star formation rates

The Hubble Deep Field observations, made with the WFPC2 in selected pointings of the Northern and the Southern hemispheres (Williams *et al.* 1996, 2000) opened the way to the study of *really* high redshift galaxies,
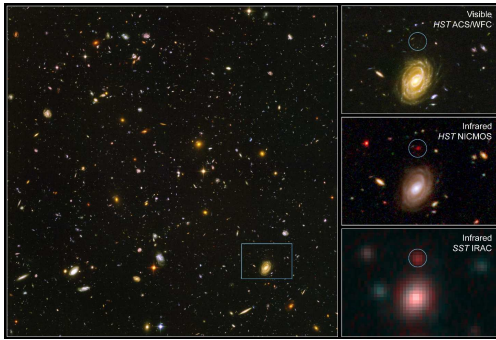
Fig. 1. The Hubble Ultra Deep Field as imaged with the *HST*-ACS. Also shown are the position, and the corresponding *NICMOS* and Spitzer-IRAC NIR images (inserts), of the massive galaxy HUDF-JD2, which is estimated to be at a redshift $z \sim 6.5$, the most distant galaxy identified in the HUDF. [Credit: B. Mobasher, NASA, ESA]

namely as high as $z \sim 5$ and just about 1.5 billion years after the Big Bang.

The original Northern hemisphere HDF revealed a population of small, irregular galaxies that often appeared in pairs or small groups. Much of the light from these objects was of high surface brightness, owing to high rates of star formation, but concentrated, requiring the resolution of HST to identify them as distant galaxies as opposed to red stars, for example. The extension of the deep-field approach to the southern hemisphere (Williams *et al.* 2000) confirmed the main conclusions of the HDF but also showed the limitations of a small field survey in drawing broad conclusions about distant populations, *i.e.* cosmic error within small fields can be substantial.

With the installation of a more efficient camera, the *ACS*, deeper and deeper studies were pursued, reaching with the Hubble Ultra Deep Field (HUDF) survey objects at redshifts as high as ~ 7 (Beckwith *et al.* 2006, Mobasher *et al.* 2005).

The Hubble Ultra Deep Field (HUDF) was conceived as a public survey, a 1 million second exposure of an 11 square-arcmin region in the southern sky imaged with the *ACS* using Director's Discretionary Time. The main science driver was galaxy evolution and cosmology, including probing the epoch of reioniza-

tion up to z~ 6.5 and characterizing not only the colors but also the morphologies of faint sources. The primary instrument was *ACS*, but *WFPC2*, *NICMOS* and *STIS* were also used in parallel.

The HUDF consists of a single ultra-deep field (412 orbits in total) within the Chandra Deep Field South (Giacconi *et al.* 2002) in the GOODS area (Giavalisco *et al.* 2004). The adopted pointing was selected so as to avoid the gaps with the lowest effective exposure on the Chandra ACIS image of CDFS. The HUDF field was also selected to be accessible to most major observatories in both Northern and Southern hemispheres.

The *ACS* exposure time was divided among four filters, F435W (B435), F606W (V606), F775W (i775), and F850LP (z850), to give approximately uniform limiting magnitudes $m_{AB} \sim 29$ for point sources. The *HST* observations were carried out between late September 2003 and mid-January 2004.

The HUDF field contains at least 10,000 objects, the vast majority of which are galaxies. Three samples of galaxies in different redshift intervals were identified in the HUDF from objects with missing flux in the shortest wavelength bands, those that "dropped out" of the B435, V606, or i775 filters, corresponding approximately to three redshift ranges, namely 3.5-4.7, 4.6-5.5, and 5.7-7, respectively. The main findings can be summarized as (Beckwith *et al.* 2006):

• Galaxies at these high redshifts are smaller and less symmetric in shape than galaxies at lower redshifts. These results confirm that galaxies evolved rapidly in the first few billion years after the Big Bang.

• The faint sources detected by the HUDF are smaller on average than the brighter objects seen in shallower surveys such as GOODS (Giavalisco *et al.* 2004) or the HDFs (Williams *et al.* 1996, 2000), with typical sizes (radius enclosing 50% of the flux) of about 0.15 arcsec.

• Although the luminosity density of galaxies at wavelengths of 1400 Å decreases modestly from redshifts of a few out to redshifts greater than 6, vigorous star formation was already un-
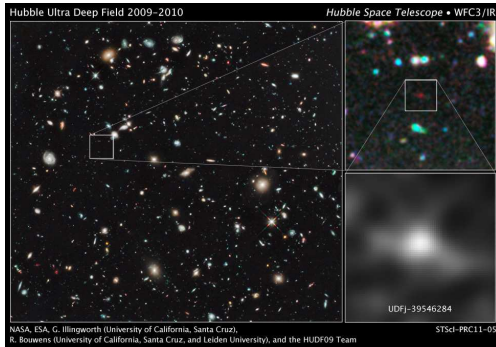
Fig. 2. Combined images of this field in the Fornax constellation, obtained with three near infrared filters of the WFC3/IR, reveal the presence of the most distant galaxy detected so far (z∼ 10). [Credit: NASA, ESA, G. Illingworth (University of California, Santa Cruz), R. Bouwens (University of California, Santa Cruz, and Leiden University), and the HUDF09 Team]
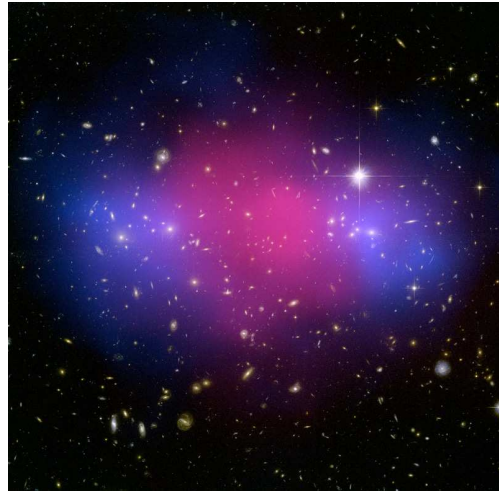

Fig. 3. *HST*-ACS and Chandra composite image of the Galaxy Cluster MACS J0025.4-1222 showing the distributions of ordinary matter (in red (around the cluster center), as mapped by its X-ray emission) and dark matter (in blue (on both sides relative to the center), detected by means of gravitational lensing measurements). [Credit: Bradac & Allen, NASA, ESA, CXC]

derway when the Universe was less then 1 billion years old.

After the installation of WFC3 in mid-May, the HUDF09 program (GO-11563) devoted 192 orbits to observations of three fields, including the HUDF, using the newly available F105W, F125W and F160W near-infrared filters (*i.e.* Y, H and J bands).

In particular, Bouwens *et al.* (2010) used a two-color Lyman-Break selection technique to identify $z \sim 8 - 8.5$ Y-dropouts, and found 5 probable candidates. The sources have H-band magnitudes of ~ 28.5 AB mag, apparent sizes of ∼0.15" ($\sim 0.7h^{-1}$ kpc), and very blue UV-continuum slopes (*i.e.* $\beta < -2.5$), suggesting that these $z \sim 8$ galaxies are not only dust free but also perhaps have very young ages or low metallicities. Follow-up deep field observations are also planned for the James Webb Space Telescope in the late 2010's.

Most recently, additional observations made by the HUDF09 team with the IR side of the WFC3 have detected a very red source that is the most distant galaxy found so far, with a photometric redshift z∼ 10 (see Fig. 6) (Illingworth *et al.*, 2011, News Release # STScI-2011-05).)

3.2. Dark matter

A powerful collision of galaxy clusters has been captured by Hubble Space Telescope and Chandra X-ray Observatory (see Figure 4). The observations of the cluster known as MACS J0025.4-1222 indicate that a titanic collision has separated the dark from ordinary matter (Bradac *et al.* 2008) and provide an independent confirmation of a similar effect detected previously in a target dubbed the Bullet Cluster (1E0657-56, Clowe *et al.* 2004, 2006, Bradac *et al.* 2006). These new results show that the Bullet Cluster is not an anomalous case. This beautiful view of the galaxy cluster MACSJ0025 demonstrates how ordinary matter and mysterious dark matter interact. The blue cloud-shaped parts flanking the centre show the position of dark matter, mapped by *HST*-ACS using gravitational lensing to measure the amount of dark matter. The red middle indicates ordinary matter, charted by NASA's Chandra X-Ray Observatory. The position of the two matter types shown in the image are ex-

Fig. 4. The central part of the 30 Doradus Nebula in the Large Magellanic Cloud, imaged by the WFC3 in the optical and near infrared. The bright group of massive stars in the upper left quadrant is the core of the 30 Dor nebula, denoted as R136. [Credit: NASA, ESA, and F. Paresce (INAF-IASF, Bologna, Italy), R. O'Connell (University of Virginia, Charlottesville), and the WFC3 Science Oversight Committee]

plained by MACSJ0025's origin. It was formed when a pair of large galaxy clusters collided. Ordinary matter in the form of hot gas slowed down and pooled at the centre but dark matter passed straight through.

4. The local Universe

4.1. Stellar populations in nearby galaxies: star formation in the Magellanic Clouds

The Magellanic Clouds (Large Magellanic Cloud, LMC, and Small Magellanic Cloud, SMC) are two dwarf, irregular galaxies, close satellites of the Milky Way. Their proximity to the MW (individual stars on the main sequence can easily be resolved and characterized with *HST* down to at least 0.5 $M_\odot$), their lower metallicities (approximately 0.4 solar for the LMC, and 0.2 for the SMC) and their high rates of star formation make them ideal sites where to study the properties of stellar popu-

lations and the prevailing processes of star formation in low metallicity environments.

In the SMC the most conspicuous region of star formation is NGC 346, which has been observed with HST in recent years (e.g. Nota *et al.* 2006, Sabbi *et al.* 2006). The properties of the young stellar populations in the field of the NGC346 cluster have been studied in detail using the detected Hα excess emission to identify pre-main sequence (PMS) objects actively undergoing mass accretion (De Marchi *et al.* 2011a, De Marchi, Panagia & Sabbi 2011). The 680 identified bona-fide PMS stars show a bimodal age distribution, with two roughly equally numerous populations peaked respectively at ∼1Myr, and ∼20Myr.

No correlation is found between the locations of young and old PMS stars, and no systematic correspondence is found between the positions of young PMS stars and those of massive OB stars of similar age. Furthermore, the mass distribution of stars with similar age shows large variations throughout the region.

An interesting implication of such separation between regions where massive stars and low-mass objects appear to form is that high-mass stars might not be "perfect" indicators of star formation and, hence, a large number of low-mass stars formed elsewhere might have so far remained unnoticed (De Marchi *et al.* 2011a). For certain low surface density galaxies this way of preferential low-mass star formation may be the predominant mechanism, with the consequence that their total mass as derived from the luminosity may be severely underestimated and that their evolution is not correctly understood.

The LMC harbors the largest star forming region of the Local Group, i.e. the 30 Doradus (30 Dor) Nebula. The detailed properties of the stellar populations in the central regions of 30 Dor, centered on a bright core, denoted as R136 (see Fig. 7), have recently been studied using observations made with the WFC3 (De Marchi *et al.* 2011b).

On the basis of a strong Hα excess emission, about 1150 PMS stars are identified over the entire field. Their locations in the Hertzsprung-Russell diagram reveal that about one third of them are younger than about 4Myr,
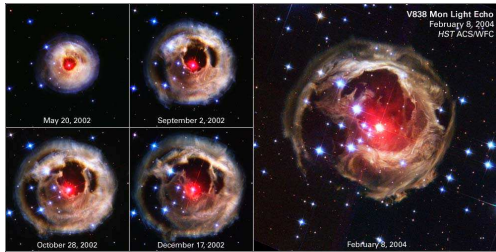
Fig. 5. Comparison of ACS images of V838 Mon obtained between May 20, 2002, and February 8, 2004. The structure is dominated by a series of nearly circular arcs and rings, centered on the variable star, but there are cavities that become progressively more asymmetric with time. [Credit: H.E. Bond (STScI), Hubble Heritage Team, NASA, ESA]

Fig. 6. Comparison of ACS images of V838 Mon obtained between November, 2005, and September, 2006. The apparently slower expansion of the echo may indicate that it has reached the outer layers of the previously ejected material. [Credit: H.E. Bond (STScI), Hubble Heritage Team, NASA, ESA]

compatible with the age of the massive stars in the central ionising cluster R136, whereas the rest have ages up to 30Myr, with a median age of about 12Myr.

While the younger PMS population preferentially resides in the central regions of the cluster, older PMS objects are more uniformly distributed across the field and are remarkably few at the very centre of the cluster. This effect is likely to be due to photoevaporation of the older circumstellar discs caused by the massive ionising members of R136.

4.2. The mysterious outburst of the star V838 Monocerotis

The previously unknown variable star V838 Monocerotis erupted in early 2002, brightening suddenly by a factor of almost 10,000 at visual wavelengths. Unlike a supernova or nova, V838 Mon did not explosively eject its outer layers, rather, it simply expanded to become a cool supergiant with a moderate-velocity stellar wind. A series of superluminally expanding ring-like structures (light echoes) appeared around the star shortly afterward, as illumination from the outburst propagateThe star and its surrounding medium has been studied through a series of high-resolution images and polarimetry of the light echo with the *HST*-ACS.

The echo exhibits a series of circular arcs, whose angular expansion rates show that the

distance is greater than 2 kpc. The polarimetric imaging (Sparks et al. 2008) shows that the distance is actually as high as 6 kpc. This distance agrees very well with that measured for the star cluster that surrounds V838 Mon (Afsar & Bond 2007). It is estimated that at maximum light, the object was extremely luminous, at least as bright as visual absolute magnitude -9.6, which is about a million times brighter than the Sun. The spectrum of the star during the outburst remained that of a cool stellar photosphere, but as the outburst subsided a composite spectrum appeared, which revealed the presence of a hot star companion.

More recent observations (see Figure 10) show that the expansion of the light echo appears to slow down suggesting that it has reached the outer layers of the previously ejected material. The corresponding radius is about 2 pc, which, adopting a physical expansion velocity similar to the observed velocity of the ejecta in 2002 outburst ($\sim 200\,\mathrm{km\,s^{-1}}$), provides an age of about 10,000 years for the last matter ejection episode before the 2002 outburst.

V838 Mon thus appears to represent a new class of stellar outbursts, occurring in binary systems containing a relatively hot main-sequence star and a companion that erupts to become a cool supergiant. A remarkably similar event was seen in the Andromeda Galaxy in the late 1980's. When combined with the
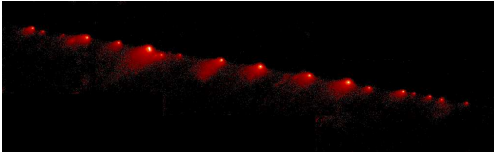
Fig. 7. A composite of several images of Comet P/Shoemaker- Levy 9 fragments taken with HST-WFPC2 in February 1994 that shows the full "string of pearls", i.e. the whole series of the comet fragments. [Credit: H.A Weaver & T.E.. Smith (STScI), NASA]
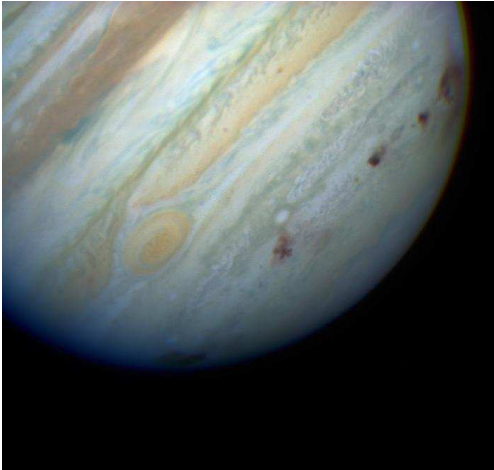

Fig. 8. Image of Jupiter taken with the HST-WFPC2 on July 22, 1994. Eight impact sites are visible. [Credit: NASA, ESA, H. Hammel (Space Science Institute, Boulder, Colo.), and the Jupiter Impact Team]

high luminosity and unusual outburst behavior, these characteristics indicate that V838 Mon represents a hitherto unknown type of stellar outburst, for which we have no completely satisfactory physical explanation.

5. Studies of Solar system objects

5.1. The impact of comet Shoemaker-Levy 9 on Jupiter

Comet Shoemaker-Levy 9 (SL9, formally designated D/1993 F2) was a comet that broke apart and collided with Jupiter in July 1994. In July 1992 the orbit of Shoemaker-Levy 9
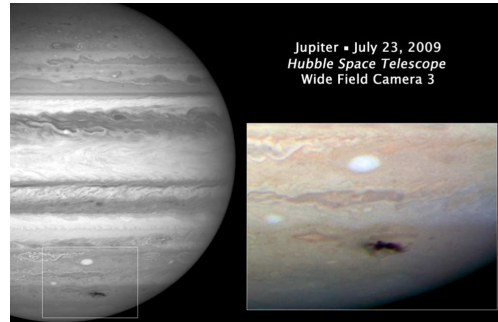

Fig. 9. A new spot on Jupiter, caused by the impact of a comet or an asteroid, was observed with HST-WFC3 on July 23, 2009. [Credit: NASA, ESA, H. Hammel (Space Science Institute, Boulder, Colo.), and the Jupiter Impact Team]

had passed within Jupiter's Roche limit, and Jupiter's tidal forces acted to pull the comet apart. SL9 was later observed as a series of fragments ranging up to 2 km in diameter, often referred to as the "string of pearls" (Fig. 11). The twenty-one large chunks of the comet collided with Jupiter's southern hemisphere between July 16 and July 22, 1994, at a speed of approximately 60 km/s. The prominent scars from the impacts were more easily visible than the Great Red Spot and persisted for many months. In particular, an *HST* image of Jupiter obtained on July 22, 1994, shows eight impact sites (see Fig. 12). These features rapidly evolved on timescales of days. The smallest features in the this image are less than 200 kilometers across.

This was the first impact ever observed in the Solar system but not the last one!

On July 23, 2009, NASA scientists interrupted the checkout and calibration of the Hubble Space Telescope to aim at a new expanding spot on Jupiter. The spot, caused by the impact of a comet or an asteroid, was discovered by the Australian amateur astronomer Anthony Wesley on July 19, 2009. The Hubble picture (Fig. 13), taken on July 23, 2009, is the sharpest image taken of the impact feature. The observations were made with *HST* new camera, the Wide Field Camera 3. Even if WFC3 was not yet fully calibrated, it is clear that the it is already able to return meaningful science
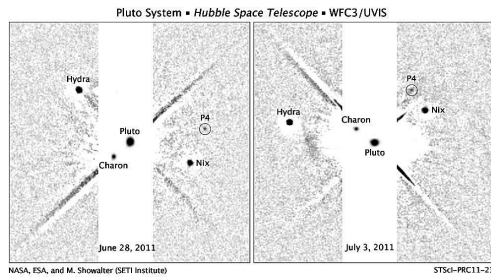
Fig. 10. Two images of Pluto and its satellites taken with the WFC3 on June 28, 2011 (left) and July 3, 2011 (right) reveal the presence of a fourth moon, dubbed P4, in addition to Charon, Hydra and Nix. [Credit: NASA, ESA, and M. Showalter (SETI Institute)]

images that can complement images taken with ground-based telescopes.

5.2. Discovery of a fourth satellite orbiting around Pluto

Another satellite orbiting the distant, icy dwarf planet Pluto has been found Hubble Space Telescope. This discovery expands the size of Pluto's known satellite system to four moons. The tiny, new satellite, temporarily designated P4, was discovered in a Hubble survey searching for rings around the dwarf planet.

The new moon is the smallest moon yet discovered around Pluto. It has an estimated diameter of 13 to 34 km. By comparison, Charon, Pluto's largest moon, is 1,200 km across, and the other moons, Nix and Hydra are in the range of 32 to 113 km in diameter.

The two images (see Figure 14), which were taken about a week apart by NASA's Hubble Space Telescope, show four moons orbiting Pluto. The green circle in both snapshots marks the newly discovered moon, temporarily dubbed P4, found by Hubble in June 2011. The new moon lies between the orbits of Nix and Hydra, two satellites discovered by Hubble in 2005. P4 completes an orbit around Pluto roughly every 31 days. The new moon was first seen in a photo taken with Hubble's Wide

Field Camera 3 on June 28, 2011. The sighting was confirmed in follow-up Hubble observations taken July 3 and July 18. These Hubble observations will help NASA's New Horizons mission, scheduled to fly through the Pluto system in 2015.

References

Afsar, M., & Bond, H.E., 2007, AJ, 133, 387
Beckwith, S.V.W., *et al.*, 2006, AJ, 132, 172
Bond, H.E., *et al.*, 2003, Nature, 422, 405
Bouwens, R.J., *et al.*, 2010, ApJ, 709, L133
Bradac, M., *et al.*, 2006, ApJ, 652, 937
Bradac, M., *et al.*, 2008, ApJ, 687, 959
Clowe, D., *et al.*, 2004, ApJ, 604, 596
Clowe, D., *et al.*, 2006, ApJ, 648, L109
Della Valle, M., Panagia, N, 1992, AJ, 104, 696
De Marchi, G, Panagia, N, Sabbi, E., 2011, ApJ, , in press
De Marchi, G, *et al.*, 2011a, ApJ, , in press
De Marchi, G, *et al.*, 2011b, ApJ, , in press
Giacconi., *et al.*, 2002, ApJS139, 369
Giavalisco M., *et al.*, 2004, ApJ, 600, L93
Mobasher, B., *et al.*, 2005, ApJ, 635, 832
Nota, A., *et al.*, 2006, ApJ, 640, L29
Panagia N., 1999, in *Frontier Objects in Astrophysics and Particle Physics*, eds. F. Giovannelli & G. Mannocchi, Italian Physical Society (Bologna - Italy), CP Vol. 65, p. 25-36.
Panagia N., 2005a, NCimB, 120, 667
Panagia N., 2005b, NCimB, 120, 897
Panagia N., 2010, Mem. S.A.It., 81, 49
Rages K., Hammel H.B., Lockwood G.W., 2002, Icarus, 159, 262
Sabbi, E., *et al.*, 2007, AJ, , 133, 2430
Sparks, W.B., *et al.*, 2008, AJ, 135, 605
Sromovsky L.A., Fry P.M., Limaye S.S., Baines K.H., 2003, Icarus, 163, 256
Williams, R.E., *et al.*, 1996, AJ, 112, 1335
Williams, R.E., *et al.*, 2000, AJ, 120, 2735